Electrochimica Acta 461 (2023) 142683

Contents lists available at ScienceDirect

Electrochimica Acta

journal homepage: www.journals.elsevier.com/electrochimica-acta

One-pot electrodeposition of multilayered 3D PtNi/polymer nanocomposite. H_2O_2 determination in aerosol phase

Rebeca Jiménez-Pérez [a], Jerónimo Agrisuelas [b], Alicia Gomis-Berenguer [c], María Teresa Baeza-Romero [d], Edelmira Valero [a,*]

[a] Department of Physical Chemistry, Higher Technical School of Industrial Engineering, Universidad de Castilla-La Mancha, Albacete 02071, Spain
[b] Department of Physical Chemistry, Faculty of Chemistry, Universidad de Valencia, Valencia 46100, Spain
[c] Faculty of Science, Institute of Electrochemistry, Universidad de Alicante, Alicante 03690, Spain
[d] Department of Physical Chemistry, School of Industrial and Aerospace Engineering, and Institute of Nanoscience, Nanotechnology and Molecular Materials, Universidad de Castilla-La Mancha, Toledo 45071, Spain

ARTICLE INFO

Keywords:
Layer-by-layer electrodeposition
3D architecture
One pot synthesis
Tunable porosity
Ionic liquid

ABSTRACT

In this work, 3D-structured nanocomposites were synthesized in one pot by electrochemical deposition of alternating layers of an *azo* type polymer (polyazure-A) with platinum and nickel nanoparticles. The hybrid PtNi/poly(AzA) film was electrochemically deposited on screen-printed carbon electrodes by layer-by-layer assembly as a function of the number of cyclic voltammograms for electrodeposition of the conducting polymer and the electrode potential applied for electro-reduction of the metal salts. The physicochemical characteristics of the resulting films were studied using electrochemical and microscopic techniques. The 3D molecular nano-architecture presents a hollow porous structure dependent on the electrode potential set for the electro-reduction of Pt and Ni nanoparticles. The electrochemical sensor was validated in terms of sensitivity, limit of detection, stability and repeatability, exhibiting a highly sensitive H_2O_2 detection, with LoD 68.5 nM ($S/N = 3$) at 0.05 V *vs.* Ag-SPCE for the electrode modified with 20 cycles for the conducting polymer electrodeposition and −2.0 V for metal ions reduction. The aim of this work also included the outcome of the electrochemical sensor after incorporating the room temperature ionic liquid 1-butyl-2,3-dimethylimidazolium tetrafluoroborate within the PtNi/poly(AzA) film, which notably improved the analytical parameters of the system, with LoD 14.5 nM at the same potential. Therefore, as proof of concept, the PtNi/poly(AzA) film-based electrode was explored towards the suitability of an electrochemical sensor for the determination of hydrogen peroxide in aerosol phase. The outstanding features of the PtNi/poly(AzA) film-based electrode modified with the aforementioned ionic liquid allowed for the continuous monitoring of H_2O_2 in an aerosol stream generated with an ultrasonic diffuser at the low applied potential of 0.05 V. In addition, monitoring H_2O_2 samples through a series of ON/OFF switches for over 3 h, the sensor provided a fast and reproducible response.

1. Introduction

In recent years, interest has grown in the design of advanced materials capable of being tuned for specific applications, with the focus being on the synthesis, characterization and functionalization of materials with hollow architectures and mesoporous nanostructure. The most recent trend is to pay attention to the development of new porous materials, including porous electrodes [1,2], hollow-structured mesoporous materials [3], hierarchical systems with interconnected pores [4], porous organic materials [5] and polymer frameworks [6].

Over the last few years, the synthesis of particulate polymeric matrix nanocomposites has attracted intense research attention since, due to their versatility, large specific surface area, ordered mesostructure, and variety of frameworks, among other factors, polymeric nanocomposites can be used for multiple purposes [7,8]. As a result of the large surface-to-volume ratio, one of the most significant applications of these nanostructured materials lies in the development of ultrasensitive sensors in the detection of analytes in vapor/gas phase [9,10]. Conducting polymer composites containing metallic or metal oxide nanoparticles have also attracted particular attention in the field of electrochemical

* Corresponding author.
E-mail address: Edelmira.Valero@uclm.es (E. Valero).

https://doi.org/10.1016/j.electacta.2023.142683
Received 3 February 2023; Received in revised form 25 May 2023; Accepted 30 May 2023
Available online 31 May 2023

sensing and, most notably, functional π-conjugated organic polymers, such as poly(azure-A), which exhibits unusual electrochemical properties [11,12]. As has been previously shown by our research group, this azo-type polymer presents excellent properties, such as high surface area, stability and electroconductivity [13–15] in addition to valuable catalytic response and biocompatibility [16]. Materials with these properties have proved promising in application prospects in various fields.

Different assembly methods have been applied to the combining of polymers and nanoparticles of noble metals [17] or transition metal oxides [18], manipulating the specific interactions in an ordered manner, to investigate the potential range of applications [19]. Electrochemical methods offer the possibility of better morphological and chemical control of nanoparticulate systems [20]. Layer-by-layer (LbL) electrodeposition is a straightforward methodology enabling the simultaneous combination of different nanocomponents to produce hybrid materials that can be deposited on a broad variety of supports [21]. With this approach, it is possible to combine properties of several types of materials and modulate their structure, as well as control thickness to develop new and specific nanocomposites. As a result of the versatility of the technique, its use has increased significantly in recent years, particularly in the assembly of inorganic nanoparticles together with polymers [22,23].

The preparation of polymeric matrix nanocomposites can be performed by the consecutive combination of potential scan for the electrosynthesis of the polymeric film coupled with the electrodeposition of the metallic electrocatalyst, using the corresponding salts under controlled potential. The above electrochemical procedure, which can be defined as LbL co-electrodeposition, yields three-dimensional (3D) templates with homogeneous distribution of the metals inside the polymeric film [24] due to: (i) direct deposition of the metal nanoparticles, (ii) the presence of oxidized metal formed during the polymerization process [7] and (iii) the partially reduced state of the metal ion, embedded in the growing polymeric matrix [25]. It has been observed that, as reported by Wysocka-Zołopa [26], morphology and redox properties of conjugated polymers are also affected by metal clusters through delocalization of π-bonding electrons of this type of metallized polymer. Additionally, this synthesis method will not only be useful for assembling inorganic nanoparticles with diverse polymers but can also be extended to address specific functions [27].

This paper examines the fabrication of a new functional hybrid polymeric nanomaterial obtained by LbL electrodeposition in one pot from an electrolytic bath containing both a precursor monomer of the redox polymer Azure A and metal salts. In particular, Pt/Ni nanoparticles (NPs) were co-deposited with the conductive azopolymeric films by consecutively coupling the polymer oxidation and metal ion reduction, using different electrodeposition potentials and varying the number of cycles in order to construct the polymeric complexes with 3D nanostructure, PtNi/poly(AzA). In this regard, using conducting poly (azure-A) as a charge-transfer medium has the advantage of tailoring its characteristics to suit any given conditions [28].

As a result of the hollow void created within the 3D-like polymer matrix nanocomposite, confinement effects using a room temperature ionic liquid (RTIL) will also be investigated to analyze the potential of these modified surfaces for H_2O_2 electrosensing at very low concentrations, in the nanomolar range. The combination of Pt/Ni nanoparticles, the nanoporous structure of the conducting polymer and the presence of the RTIL have demonstrated high stability and reproducibility, as well as enhanced current response at the low oxidation potential of 0.05 V for H_2O_2 detection. Finally, the modified electrode was successfully applied for the real-time monitoring of H_2O_2 released from an ultrasonic diffuser in aerosol phase as a first step towards evaluating its suitability for air samples, with excellent results.

The development of techniques to measure H_2O_2 in the aerosol phase is currently under great demand for many reasons, including its role as a biomarker in breath analysis for the detection of respiratory diseases [29] and for the detection of peroxide-based explosives [30]. It is also a widely used indoor disinfectant and sterilizing agent (especially since the COVID-19 pandemic [31]) and is commonly used as an additive in water for crop irrigation to increase the dissolved oxygen concentration and so increase the ability of plants and roots to absorb nutrients from the soil [32], as well many other applications. Additionally, measuring H_2O_2 in atmospheric aerosols is of great importance because it is a key oxidant and provides insight into the oxidative potential of atmospheric particles, which has implications for human health and climate change [33].

2. Experimental

2.1. Materials

Azure A (80%), potassium hexachloroplatinate (IV) (≥99.99%), H_2O_2 (35%), nickel (II) acetate tetrahydrate, sodium dodecyl sulfate (SDS 95%), 1-butyl-2,3-dimethylimidazolium tetrafluoroborate ([BDMIM][BF_4]), N,N-dimethylformamide (DMF) (99%) and titanium (IV) oxysulfate (1.9–2.1%) for determination of hydrogen peroxide (according to DIN 38 409, part 15 DEV-18) were purchased from Sigma-Aldrich. KH_2PO_4, K_2HPO_4 and $K_4[Fe(CN)_6]$ were acquired from Merck and KNO_3 from Fluka. All the chemicals were of analytical grade and of the highest purity available. Liquid oxygen solution for plants (aqueous 11.9% hydrogen peroxide solution) was purchased from Growth Technology (Taunton, UK). H_2O_2 solutions were freshly prepared, and their concentration was checked by measuring the absorbance at 240 nm ($\varepsilon = 43.6\ M^{-1}\ cm^{-1}$) [34]. The electrodes herein used as support were disposable screen-printed carbon electrodes (SPCEs, DRP-110) from Metrohm DropSens (Spain).

2.2. Synthesis of PtNi/poly(AzA) film by LBL electrodeposition

After a first step of SPCE electrochemical activation [35], poly(azure A) (poly(AzA)) containing platinum/nickel-nanoparticles was electrodeposited, using the one-pot approach. Firstly, a poly(AzA) layer was electrodeposited onto the SPCE working electrode in an aqueous solution containing 0.02 M SDS, 1 mg/ml monomer azure A, 3.2 mM K_2PtCl_6 and 3.2 mM $Ni(CH_3CO_2)_2{\cdot}4\ H_2O$ by cyclic voltammetry (CV). The initial potential was set to +0.5 V with a potential window between +1.0 V and −0.25 V *versus* Ag-SPCE (scan rate 0.01 V/s). After running each cycle, the electrodeposition of Pt/Ni-nanoparticles then took place onto the poly(AzA) layered electrode by applying a constant potential for 30 s. The reduction potentials tested in this work were −0.5, −1.0, −1.5 and −2.0 V. Such electrodeposition sequences were alternately repeated 5 or 20 times to prepare the nanocomposite with the as-desired number of PtNi/poly(AzA) layers.

2.3. Characterization of the modified SPCE electrodes

CV, chronoamperometry and electrochemical impedance spectroscopy (EIS) experiments were performed using an AUTOLAB PGSTAT 128 N (Eco Chemie B.V.) equipped with a frequency response analyzer (FRA) module controlled by the NOVA 2.0 software package.

The one-pot electrodeposition process and the evaluation of the films formed were gravimetrically monitored using an electrochemical quartz crystal microbalance (EQCM), Metrohm AUTOLAB, with AT-cut piezoelectric quartz crystals (Au/TiO_2 crystal) with 6 MHz resonance frequency. The EQCM was calibrated following the methodology in Ref. [36]. The experimental Sauerbrey's constant obtained was $2.0294{\cdot}10^8\ Hz{\cdot}g^{-1}{\cdot}cm^2$. The EQCM system for preparation and investigation of the properties of the nanocomposite was completed with a 3 M Ag/AgCl reference electrode and a platinum counter electrode.

For high-resolution images of the modified surfaces, a Zeiss high-resolution scanning electron microscope (HRSEM) operating at 2.00 kV under high vacuum conditions was used. For SEM cross section

images, the electrodes were cut with pincers to ensure an even cut. TEM images were taken using a JEOL JEM-1400 Plus microscope (JEOL, Akishima, Tokyo, Japan) working at 120 kV. For this analysis, the surface of the electrodes was scraped and samples were dispersed in absolute ethanol, dropped onto a Lacey-covered copper grid and evaporated in the air at room temperature.

X-ray photoelectron spectroscopy (XPS) was performed using a K-Alpha spectrometer (Thermo Scientific, Waltham, MA, USA). Each spectrum was recorded using Al-Kα radiation (1486.6 eV), and monochromatized by a twin crystal monochromator, generating a focused X-ray spot with a diameter of 400 nm, at 3 mA × 12 kV. The alpha hemispherical analyzer was set to the constant energy mode with survey scan pass energies of 200 eV to access the whole energy band and 50 eV in a narrow scan.

Spectrophotometric measurements were taken by a UV/Vis Perkin-Elmer Lambda 35 (PerkinElmer Instruments, Waltham, USA) spectrophotometer. The titanium (IV) oxysulfate solution was added to H_2O_2 samples and the absorbance was measured at 407 nm [37].

2.4. H_2O_2 sensing in aerosol phase

The modified SPCEs with PtNi/poly(AzA) were electrochemically tested for the determination of H_2O_2 in aerosol phase. For this purpose, H_2O_2 solutions in phosphate buffer (PB) were atomized, using a common ultrasonic oil/water diffuser. The modified SPCE was held at 2 cm from the outlet of the atomized stream (Scheme 1). Before the measurement, the electrode surface was moistened with 10 μL PB. The diffuser, which initially contained PB, was then immediately turned on. Once the steady current was reached, H_2O_2 at the desired concentration was injected into the system with a Hamilton syringe through a septum.

3. Results and discussion

3.1. Electrodeposition of Pt and Ni into the conductive polymer

Hybrid nanocomposites PtNi/poly(azure A) were obtained by electrodeposition of an initial poly(AzA) thin film by CV on a previously activated SPCE, followed by the cathodic electrodeposition of the metallic nanoparticles, from a bath containing both the monomer azure A and the metal salts. This procedure was performed multiple times to produce the multilayered nanocomposite. The potential range for the poly(AzA) formation, the cathodic potential for Pt/Ni electrodeposition and the number of cycles are key factors to control the amount of material deposited and notably influence the physicochemical and morphological features of the new surfaces developed, and so must be fine-tuned [38].

Therefore, a set of experiments were first carried out, using CV to establish the most adequate conditions for the layer-by-layer electrosynthesis of the hybrid nanocomposite in one pot. The potential window typically used for the polymerization of AzA [39] was herein extended to check for subsequent oxidation of either Pt or Ni nanoparticles, since that would lead to re-dissolution of metals back into the bath. Fig. 1 shows the voltammetric responses obtained in the presence of AzA and SDS solutions in the absence of metal salts (CV a), in the presence of 3.2 mM Ni(II) (CV b), 3.2 mM Pt(IV) (CV c) and simultaneous presence of both salts at the same concentration (CV d). Plot *a* displays the typical profile of poly(AzA) synthesis in SDS, which has previously been shown to provide the polymer with better electrocatalytic properties than other inorganic anions, as well as special sensitivity to the electrocatalysis of H_2O_2 [39,40]. Plots *b* and *c* correspond to the CVs obtained when the metallic salts were individually present, in which the cathodic peaks associated with the reduction of $Ni(CH_3CO_2)_2$ and K_2PtCl_6 can be appreciated, close to −1.4 V and −0.5 V, respectively. Both scans simultaneously exhibit an increase in the current at the highest reduction potentials. Finally, plot *d* shows the curve obtained when both Pt and Ni salts were simultaneously added into the electrolyte solution. A marked cathodic current was noticed at negative potentials starting from −1.0 V, related to hydrogen evolution together with the electrodeposition of Ni, whilst the peak at −0.45 V was attributed to $PtCl_6^{2-}$ reduction [41]. The voltammetric response displayed in *d* also shows an unusual crossed voltammogram, where the anodic scan crosses over the reverse scan within the potential range of −1 V and −2 V. This noteworthy feature has been extensively studied in the literature, being associated with electrochemical nucleation when active sites are present in a 3D structure [42].

Therefore, and according to Fig. 1, applied potentials for the electroreduction step of Pt/Ni were first established at −0.5, −1.0, −1.5 and −2.0 V, with a potential pulse duration of 30 s, whereas the number of CV cycles was set at 5 and 20 with a potential window between +1.0 V and −0.25 V, in order to explore the electrochemical response of the PtNi/poly(AzA) films on hydrogen peroxide oxidation. Consequently, a total of eight PtNi/poly(AzA) films were prepared (see processing in Table 1).

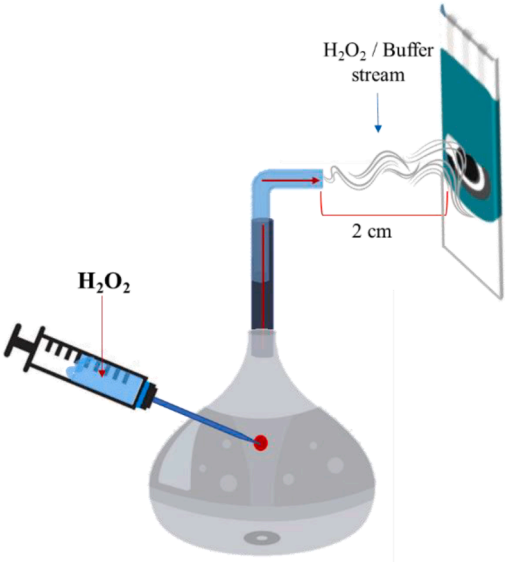

Scheme 1. Experimental setup for generation and electrochemical detection of H_2O_2 in aerosol phase.

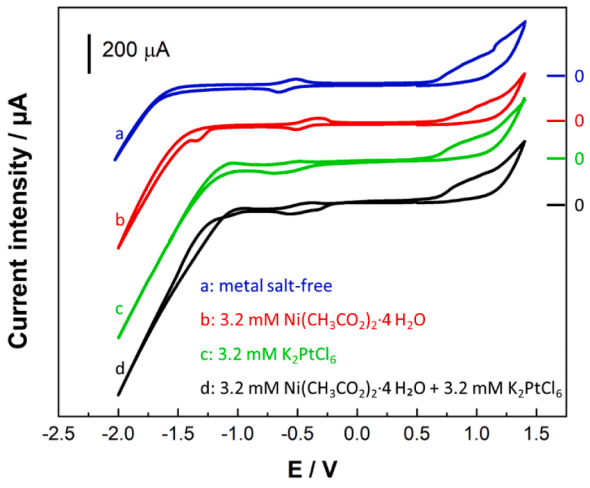

Fig. 1. Cyclic voltammograms obtained in azure A (SDS) aqueous solutions between 1.5 V and −2.0 V. The voltammetry cycle was started at 0.5 V. Scan rate: 10 mV s^{-1}.

Table 1
ΔE_P and R_{ct} values obtained by CV and EIS for the different polymeric films herein obtained.

PROCESSING			CV	IMPEDANCE	PROCESSING			CV	IMPEDANCE
CV Cycles	Potential applied (V)	Electrode number *	ΔE_P (V)	R_{ct} (Ω)	CV Cycles	Potential applied (V)	Electrode number*	ΔE_P (V)	R_{ct} (Ω)
5	−2.0	1	0.093	307	20	−2.0	2	0.123	1262
5	−1.5	3	0.115	450	20	−1.5	4	0.137	1969
5	−1.0	5	0.125	490	20	−1.0	6	0.140	4857
5	−0.5	7	0.128	560	20	−0.5	8	0.193	6067

* Electrode number as indicated in the legend to Fig. 2.

3.2. Electrochemical characterization

Fig. 2A reports the CV response of the PtNi/poly(AzA) electrodes in the presence of the redox probe $K_4[Fe(CN)_6]$ as a function of the number of CV cycles and reduction electrode potentials. The solid lines show the CVs obtained upon 20-layer nanocomposites, PtNi/poly(AzA)−20*l*, while the dotted lines (inset) display the CVs obtained with those of 5 layers, PtNi/poly(AzA)−5*l*. In both cases, the highest peak current intensities for the redox couple and the fastest redox kinetics (with lower ΔE_P values, see Table 1) were obtained when the electrodeposition of metals Pt/Ni took place at −2.0 V, which indicates the presence of a larger number of reactive sites in these electrodes [43].

The growth of the PtNi/poly(AzA) nanocomposite film was also evaluated by electrochemical impedance spectra (EIS) analysis. Fig. 2B depicts the EIS spectra obtained in a frequency range from 0.1 Hz to 20 kHz by applying 0.125 V, fitted to the Randles circuit (inset) [44,45]. The R_{ct} values varied from 307 Ω to 560 Ω for PtNi/poly(AzA)−5*l* electrodes and between 1262 and 6067 Ω for PtNi/poly(AzA)−20*l* electrodes (Table 1). The trend of ΔE_P and R_{ct} values was markedly influenced by the reduction potential applied in the construction of the nanocomposite. It was observed that the more negative the potentials applied were, the more the electrical conductivity improved, as indicated by peak currents, ΔE_P and R_{ct} values (Fig. 2A and 2B).

For further evaluation, the electron transfer rate constant, k^0, of the different modified electrodes was determined from the R_{ct} values obtained from EIS data, using the following well-known Eq. (1) [46]:

$$R_{ct} = RT/n^2F^2ACk^0 \quad (1)$$

where R_{ct} is the charge transfer resistance, R is the universal gas constant, T is the absolute temperature, n is the number of electrons transferred, F is the Faraday constant, A corresponds to the area of electrode (see Table S1 in the Supplementary Data) and C is the concentration of the redox probe $K_4[Fe(CN)_6]$. The k^0 values obtained for the PtNi/poly(AzA)−20*l* electrodes were found to vary from $1.27{\cdot}10^{-4}$ cm·s^{-1} for the electrodes generated when −0.5 V was applied for the metal ion reduction steps, to $3.40{\cdot}10^{-4}$ cm·s^{-1} for the electrodes generated by applying −2.0 V in these steps (Table S1).

All these results, taken together, suggest a high surface area morphology linked to porous electrodes and 3D electroactive features, as proposed by several authors [47,48]. From Tables 1 and S1, it can be concluded that the surfaces are more conductive (increased heterogeneous electron transfer rate) as the potential applied during the electrodeposition of metals was more negative.

3.3. Surface characterization. High resolution scanning electron microscope (HRSEM) and X-ray photoelectron spectroscopy (XPS)

The PtNi/poly(AzA)−20*l* electrodes obtained by applying −0.5 V (Fig. 3A) and −2.0 V (Fig. 3B and 3C) in the electro-reduction steps were characterized by HRSEM. Depending on the reduction potential applied, nanocomposites display significantly different morphologies according to the images. Fig. 3A depicts a smoother, more uniform film with less roughness and a compact and homogeneous surface. In contrast, Fig. 3B verifies the presence of a 3D network within the polymeric matrix filled with nanoporous cavities. The presence of metallic nanoparticles embedded in the polymeric matrix can also be clearly observed in Fig. 3C. Pore distribution and inorganic nanoparticle size were also analyzed. Fig. S1 shows pores ranging from 36 to 140 nm in diameter and a metal nanoparticle size in the order of ~20 nm. Considering the difference in morphology of the two nanocomposites and taking into account the results previously obtained through CV and EIS, it is possible

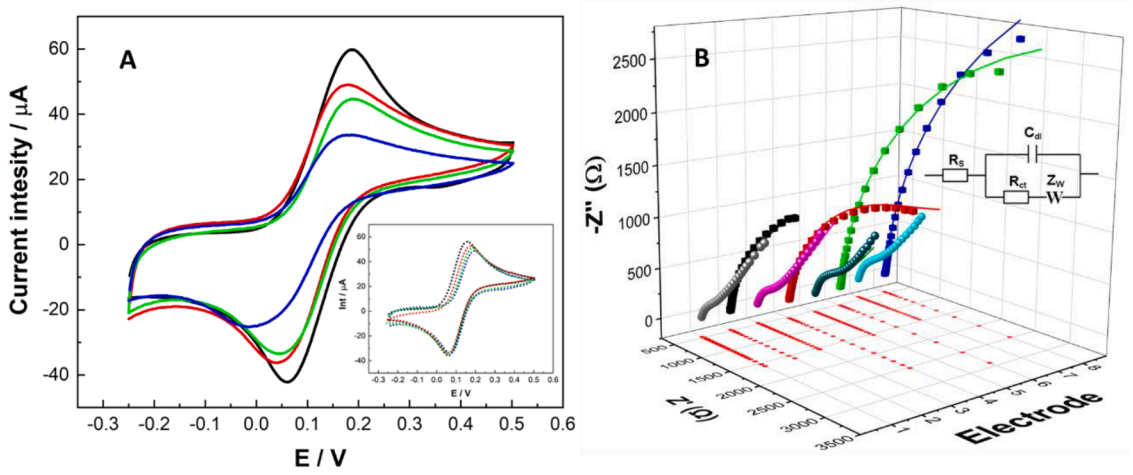

Fig. 2. (A) CVs obtained in 0.1 M KNO_3 containing 5 mM $K_4[Fe(CN)_6]$ for the surfaces constructed by applying twenty (solid lines) or five cycles (dotted lines, inset) and four negative potentials: −2.0 V (black), −1.5 V (red), −1.0 V (green) and −0.5 V (blue). Scan rate: 20 mV·s^{-1}. (B) EIS spectra of the aforementioned surfaces obtained at 0.125 V. Electrodes: 1_gray: −2.0 V/PtNi/poly(AzA)−5*l*; 2_black: −2.0 V/PtNi/poly(AzA)−20*l*; 3_pink: −1.5 V/PtNi/poly(AzA)−5*l*; 4_red: −1.5 V/PtNi/poly(AzA)−20*l*; 5_dark green: −1.0 V/PtNi/poly(AzA)−5*l*; 6_light green: −1.0 V/PtNi/poly(AzA)−20*l*; 7_light blue: −0.5 V/PtNi/poly(AzA)−5*l*; and 8_dark blue: −0.5 V/PtNi/poly(AzA)−20*l*

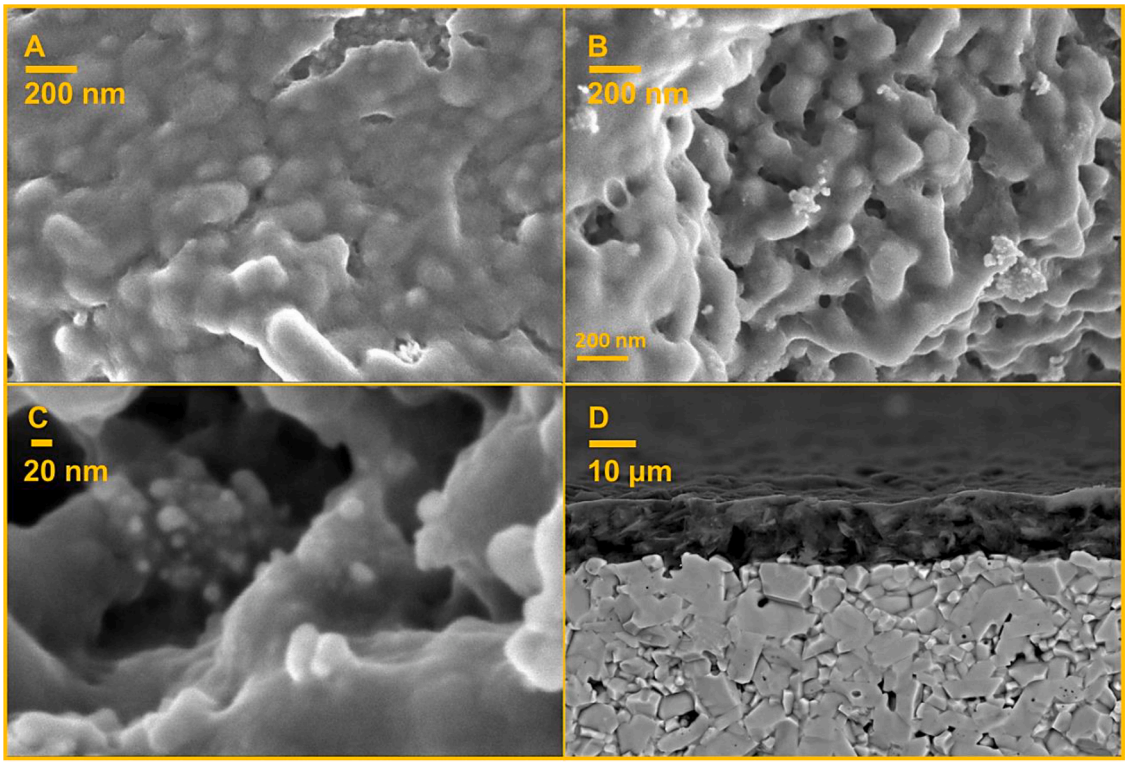

Fig. 3. HRSEM images of the polymeric films obtained at two different reduction potentials: −0.5 V (A) and −2.0 V (B and C). HRSEM cross-section image of −2.0 V/PtNi/poly(AzA)−20*l* film over the ceramic electrode support (D).

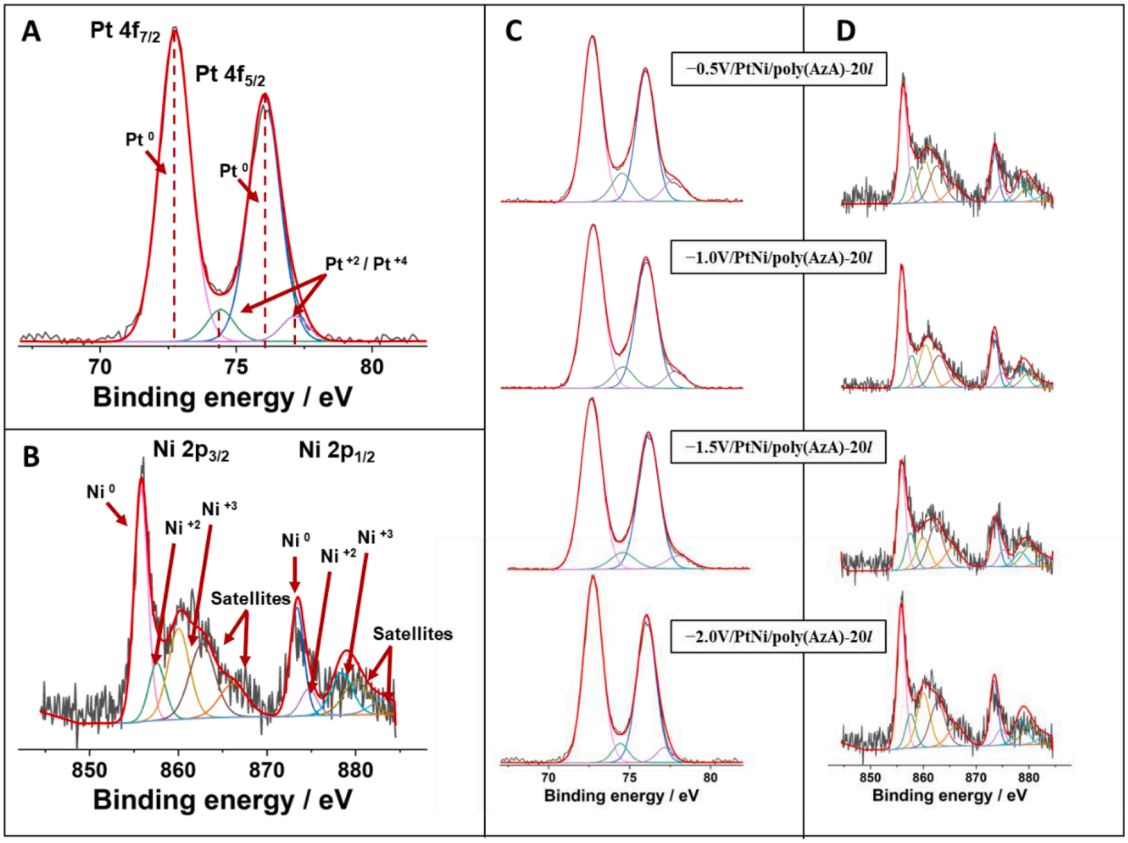

Fig. 4. High-resolution XPS spectra of Pt (4f) (A) and Ni (2p) (B), and the corresponding difference spectra after subtracting the metallic contribution. Evolution of platinum (C) and nickel (D) XPS peaks for the surfaces studied.

to conclude that the deposition of Pt and Ni particles inside the 3D polymeric structure is more efficient when the potential applied in the reduction step is −2.0 V, which will improve the electrochemical performance of the resulting nanocomposite. Fig. 3D shows a cross-sectional image of the electrode obtained at −2.0 V, supported on the ceramic substrate. From this image, the multilayer thin film is approximately 13 μm thick on average. Fig. S2 shows two TEM micrographs of this surface obtained by scraping the working electrode at two different magnifications.

To track the distribution of metal nanoparticles, EDS imaging and elemental mapping were performed. As shown in Fig. S3, Pt and Ni nanoparticles were homogeneously dispersed in the coatings. As can be seen, the application of more negative potentials for the reduction steps led to an increase in the quantity of nanoparticles deposited for both metals.

The surface chemical states of the two metals were also analyzed by XPS for PtNi/poly(AzA)−20*l* obtained by applying the four reduction potentials previously indicated. The deconvoluted spectrum of Pt 4f reveals that the binding energies of the Pt $4f_{7/2}$ and Pt $4f_{5/2}$ peaks appear at about 72.7 and 74.4 eV, respectively (Fig. 4A), which indicates the preferential formation of metallic platinum. Nonetheless, the peaks at ~74.5 and ~77.2 eV, corresponding to the oxidized states of Pt, prove an important contribution of the formation of Pt^{2+} and Pt^{4+} in all the electrodes [15]. The XPS spectra displayed in Fig. 4C show the change in the profile of the binding energies as a function of the potential applied for the reduction of metal ions. The binding energies move up-shift as the applied reduction potential is less negative, resulting in a pronounced asymmetry due to an increase in the Pt^{4+} contribution [49]. This evolution suggests the preferential formation of Pt^{2+} to the most negative potentials.

The Ni XPS spectra of the composites are shown in Fig. 4B and D. The peaks corresponding to the binding energies linked to Ni^0 (~855 and ~873 eV) revealed that the main contribution to the spectrum is related to the zero-oxidation state (Fig. 4B) [50]. Furthermore, other oxidation states were clearly present on these surfaces depicted by the peaks fitted at ~857 (Ni^{2+}) and ~860 eV (Ni^{3+}) in Ni $2p_{3/2}$, and ~874 (Ni^{2+}) and ~878 eV (Ni^{3+}) in Ni $2p_{1/2}$ core level [51]. As shown in Fig. 4D, no significant changes were observed for the four potentials applied, except for an increase in the peaks at 855 and 873 eV in −2.0 V/PtNi/poly(AzA)−20*l* electrode, ascribed to the preferential formation of Ni^0.

The morphological and electrochemical characteristics of −2.0 V/PtNi/poly(AzA)−20*l* made this electrode the most suitable option for sensing applications. Hereafter, only the nanocomposites thus obtained will be termed PtNi/poly(AzA).

3.4. Electrochemical quartz crystal microbalance (EQCM) monitoring

The EQCM was employed to monitor the growth of the hybrid films using an AzA solution containing Pt and Ni salts. The electropolymerization of AzA was performed by CV in a potential window between −0.25 V and 1.0 V, with 0.5 V as the initial and final potential, followed by the application of a constant potential of −2.0 V for 30 s for the metal nanoparticles deposition. To understand the hybrid composite formation, we shall separately analyze poly(AzA) and nanoparticle formation.

Fig. 5A (black line) shows a representative and typical CV of poly(AzA) electrogeneration [52,53]. As can be seen, the polymer was deposited on the electrode surface between 0.7 V and 1.0 V since mass increased in this potential interval (red line). At these potentials, AzA monomers are oxidized to radical cations that react to each other to form the polymeric film on the electrode surface. As the film formed is oxidized, anions in solution will incorporate into the polymer structure to keep the electroneutrality, also contributing to the mass increase. The observed electrochemical response between 0.20 and −0.25 V corresponds to the redox activity of the deposited film, which induces mass changes in this potential interval [53]: the reduction of the film from 0.20 to −0.25 V drives a loss of mass due to the expulsion of anions, whereas the oxidation of the film from −0.25 to 0.2 V recovers the mass by insertion of anions to maintain the electroneutrality inside the film. The anions exchanged are difficult to identify since the electrolyte solution is composed of dodecyl sulfate, acetate and hexachloroplatinate anions. In any event, the polymerization was unaffected by the metal salts in solution because the growth of poly(AzA) in the absence of these salts showed similar mass responses under the same experimental conditions (Fig. S4).

When the potential is changed from 0.5 V (the CV endpoint) to −2.0 V (the potential used for Pt/Ni electrodeposition), the amount of charge consumed depends on several simultaneous electrochemical processes: i) the electrodeposition of Pt/Ni nanoparticles by reduction of their corresponding ions in solution [20,54], ii) the reduction of poly(AzA)

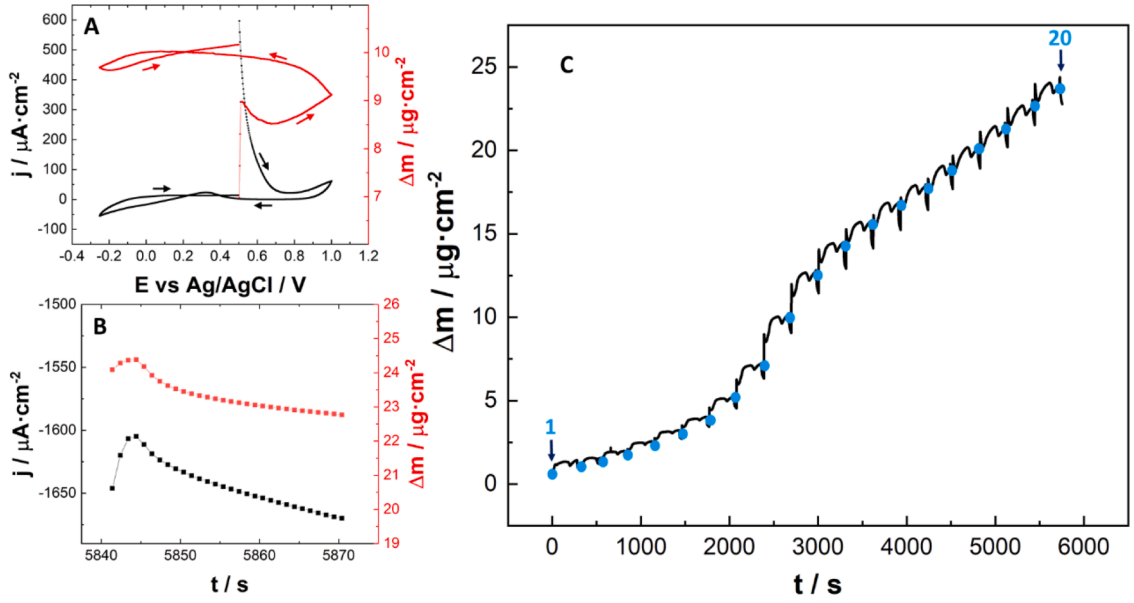

Fig. 5. (A) Representative cyclic voltammogram and (B) amperometric signal at −2.0 V plotted alongside the EQCM responses (black: current, red: mass) obtained during polymerization LbL of AzA in SDS solution containing 3.2 mM $Ni(CH_3CO_2)_2$ and 3.2 mM K_2PtCl_6. C) Mass evolution during the construction of PtNi/poly(AzA) film; the blue dots represent the increase in mass after each layer is formed. The arrows indicate the number of the layer.

[53,55], iii) the reduction of monomers in solution, and iv) hydrogen evolution. It is expected that the last two processes involve no significant mass change on the EQCM electrode.

Fig. 5B shows current (black line) and mass evolution (red line) when −2.0 V was applied for 30 s. As can be seen, mass increased during the first 4 s through preferential metal electrodeposition, then decreasing due to poly(AzA) reduction during the remaining 26 s. This is because, at this negative potential, poly(AzA) was being reduced, involving anion expulsion and proton insertion [53], with anions having a greater mass than protons.

Fig. 5C shows the mass evolution during the growth in PtNi/poly (AzA) composite for 20 steps. We observed a slow rate of deposition in the first steps that increased as the composite was accumulated on the EQCM electrode. Finally, the mass increased up to ~24 μg•cm^{-2} as the polymer and nanoparticles were deposited on the electrode surface.

3.5. Tunable morphology of the as-prepared 3D nanocomposites

The 3D nanostructure of the polymeric matrix can be usefully employed to tailor morphology and electrocatalytic activity, aiming to improve the sensitivity and selectivity of the nanocomposite to enhance the performance of the modified surface. The literature reports that ionic liquids (ILs) confined within nanopore networks manifest an anomalous enhanced efficiency, with multiple applications [56,57]. This increase in the performance has been extensively studied by computer simulation and has been interpreted in terms of confinement of the ions and interactions between ILs and pore walls. This is accompanied by partial desolvation of ions [58] as well an increase in diffusion coefficients [59]. Other authors have pointed to the existence of "superionic states" within nanopores, which indicates an easier packing of ions of the same sign [60,61]. Several studies have also demonstrated that ILs can self-assemble in a systematic order at electrode interfaces, with a significant impact on their electrochemical behavior [62–64].

This was the motivation for performing a series of tests with [BDMIM][BF_4] to study its possible effect on the electrocatalytic properties of the nanocomposite. To this end, the modified electrodes were immersed in the RTIL solution (0.5 mg IL in 1 mL DMF) and a CV was then recorded.

Fig. 6A compares the CV response of the IL-treated electrodes with that of PtNi/poly(AzA) in $K_4[Fe(CN)_6]$. The highest peak current densities and the fastest redox kinetics were obtained in IL/PtNi/poly(AzA). The heterogeneous electron transfer rate constant k^0 for the electrodes thus obtained was also calculated using Eq. (1). A value of $3.96{\cdot}10^{-4}$ cm·s^{-1} was found, which is higher than that obtained for the same electrode in the absence of the IL (Table S1). The electrodes were then tested by linear scan voltammetry in H_2O_2 solution to check their suitability for H_2O_2 detection (Fig. 6B). Electroactive features for the adsorbed IL confined in the pores exhibited the best electrochemical responses. The H_2O_2 signal could be observed at potentials even below 0.2 V in both cases, which will considerably minimize the effect of possible interfering species in real samples. The current intensity was significantly higher on IL-treated surfaces (orange line) than on non-treated ones. Additionally, it is possible to notice a slight shift of the oxidation peak potential towards even fewer positive values for IL/PtNi/poly(AzA). Compared with previous tests, the values of ΔE_P and R_{ct} (Table S2) for IL-treated electrodes demonstrated even better electrical conductivity.

3.6. Analytical performance of PtNi/poly(AzA) for the determination of hydrogen peroxide

Fig. 7A shows the calibration curves of current intensity *vs* H_2O_2 concentration for PtNi/poly(AzA) electrodes, measured at four different potentials: 0.3 V (black), 0.2 V (red), 0.1 V (green) and 0.05 V (light blue). The best signal was obtained for the experiments performed at 0.3 V and 0.2 V, with a linear range from 50 nM to 500 μM, followed by the curves at 0.1 V and 0.05 V (linear ranges from 100 nM to 500 μM and 250 nM to 500 μM, respectively). Sensitivity decreased from 51.15±0.09 nA/μM at 0.3 V to 3.28±0.06 nA/μM at 0.05 V *vs.* Ag-SPCE. However, it was possible to increase the sensitivity up to 19.22±0.08 nA/μM at 0.05 V with a quick, simple treatment with an RTIL as previously explained (dark blue line). The limit of detection (LoD) obtained at this potential for PtNi/poly(AzA) was 68.5 nM ($S/N = 3$), while it was 14.5 nM for IL/PtNi/poly(AzA). Chronoamperograms obtained by adding different concentration ranges of H_2O_2 for this last electrode are shown in Fig. 7B.

Five PtNi/poly(AzA) nanocomposites synthesized on different days over the course of a month showed a high level of reproducibility with a relative standard deviation (RSD) value of 3.2%. These electrodes can be stored (before or even after use) in dry conditions at room temperature for at least two months with no change in their analytical response. Furthermore, the proposed sensor exhibited high signal stability during the measurement, enabling continuous monitoring of H_2O_2 over time with an RSD of 1.9% in long measurements for more than 3 h. It was possible to reuse the electrodes for H_2O_2 sensing up to ten times and/or a total use time of 15 h by simply rinsing them with water.

Table S3 shows a comparison of the main analytical parameters for different PtNi-based electrodes towards H_2O_2 detection. Based on this information, we can conclude that the proposed IL/PtNi/poly(AzA) performed excellently when compared with other previously reported sensors, especially considering it is a normal screen-printed carbon

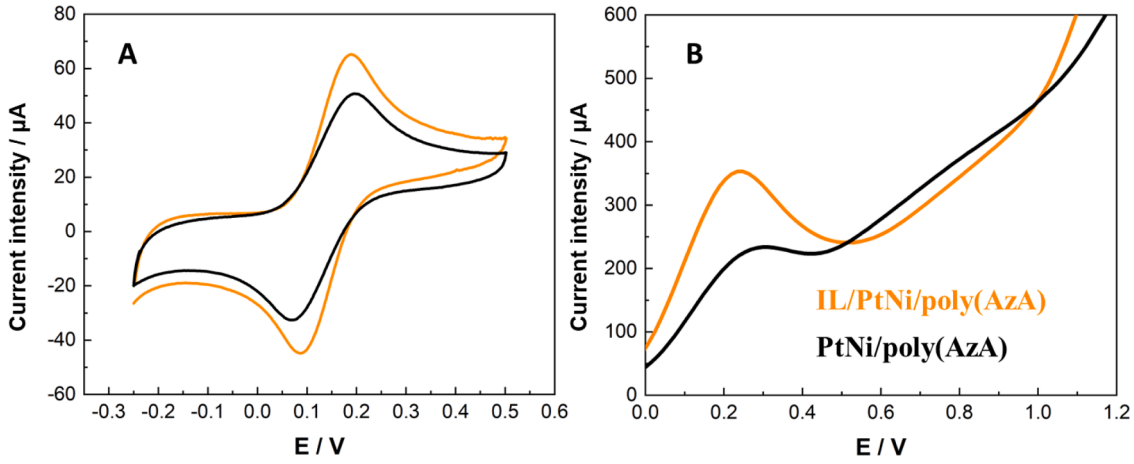

Fig. 6. Electrochemical characterization of PtNi/poly(AzA) and IL/PtNi/poly(AzA). (A) CVs obtained in 0.1 M KNO_3 containing 5 mM $K_4[Fe(CN)_6]$. Scan rate: 20 mV·s^{-1}. (B) LSVs performed in 0.1 M PB containing 10 mM H_2O_2. Scan rate: 50 mV·s^{-1}.

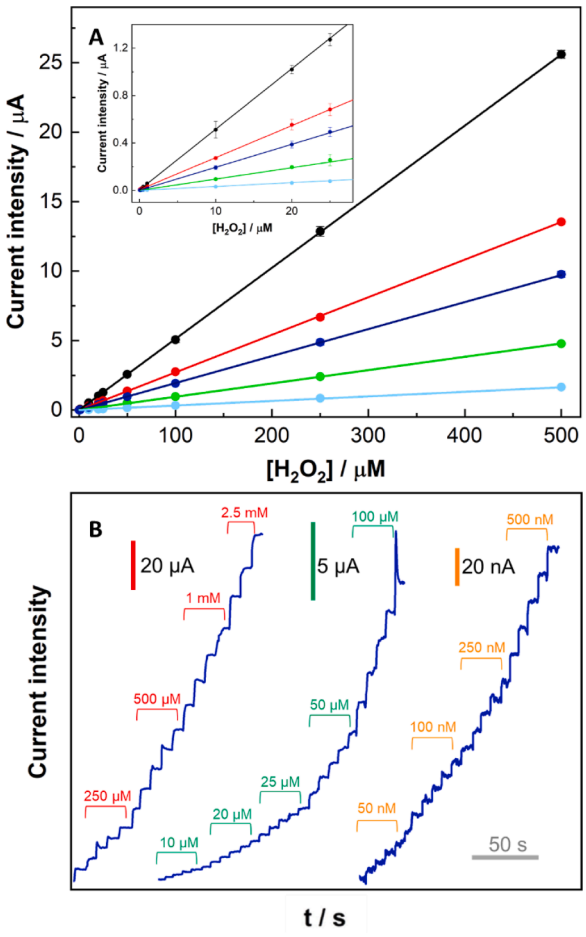

Fig. 7. (A) Calibration plots obtained by amperometry corresponding to H_2O_2 sensing in PB with PtNi/poly(AzA) electrodes under stirring conditions. Inset: magnification of the calibration curves in the lower concentration range. (B) Chronoamperometric response of IL/PtNi/poly(AzA) at three different H_2O_2 concentration ranges. Red: high concentration range, green: medium concentration range, orange: low concentration range. $E_{applied}$ = 0.05 V *vs* Ag-SPCE.

electrode. Moreover, IL/PtNi/poly(AzA) is easy to manufacture, reusable and low-cost.

3.7. H_2O_2 monitoring in aerosol phase

H_2O_2 detection and continuous monitoring in aerosol phase was performed by exposing the IL/PtNi/poly(AzA) sensor to an aerosol stream generated with a commercial ultrasonic diffuser. Once a steady current was attained under a continuous flow of PB, a known concentration of H_2O_2 was injected into the diffuser through a septum. The sensor showed a very fast response (<10 s since the addition of H_2O_2 to the diffuser) until a linear increase was obtained with time (Fig. 8). The same measurement was performed with a real sample of "liquid oxygen" for plants (an aqueous solution of H_2O_2 11.9%, appropriately diluted to attain the same concentration inside the diffuser). The results were very similar to those obtained with analytical-grade H_2O_2 and corroborate the excellent reproducibility of the sensor.

To check the results obtained with the electrochemical sensor, a well-known standard colorimetric method involving Titanium (IV) oxysulfate [65] was used to measure the same samples at the same time. This compound forms a yellow complex upon reaction with H_2O_2, which facilitates the latter's determination by spectrophotometric methods. For this purpose, a diluted peroxide stream generated with the diffuser was focused onto 50 ml water by means of a gas trap under agitation (see Scheme S1 in the Supplementary Data). Samples were withdrawn at

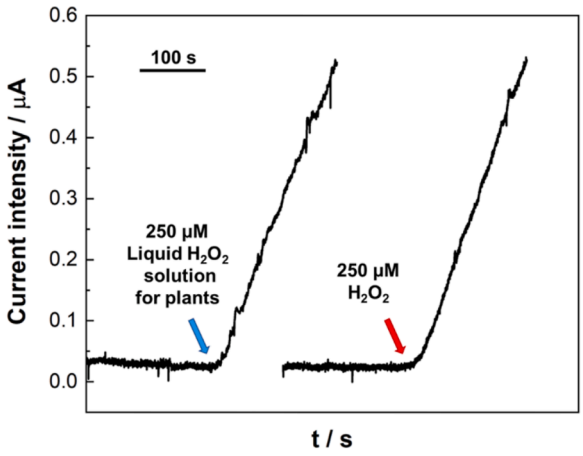

Fig 8. Real time chronoamperometric response obtained after the addition of 250 µM H_2O_2 (analytical grade (right) and liquid oxygen solution for plants (left)) into the diffuser pre-loaded with 100 mL 0.1 M PB. $E_{applied}$ = 0.05 V *vs* Ag-SPCE.

different times and were simultaneously measured using the two techniques (Fig. S5). Note that the LoD obtained with the spectrophotometric method was significantly higher (2.2 µM, Fig. S6) than that obtained with the electrochemical sensor (Fig. 7A), which is consistent with data from the literature [37] and means that the lowest H_2O_2 concentrations (< 7.5 µM) could only be determined by the electrochemical method. Using both methods, the H_2O_2 sensing results differed by less than 2.8%.

A simple comparison of the two methods indicates the main advantages of the electrochemical *vs* the colorimetric method: 1) it allows for continuous real-time measurement of the H_2O_2 signal, 2) it presents a fast response time (< 10 s), and 3) the lower H_2O_2 concentration required to induce a change in the electrochemical signal, which is clearly reflected in the values of LoD obtained.

Furthermore, the electrochemical sensor was also tested to check the possibility to make multiple accurate spot measurements over long periods with the same electrode (Fig. 9). Once a steady current was reached in phosphate buffer, a series of ON/OFF switches of the diffuser loaded with H_2O_2 500 µM in PB were conducted. Each time the diffuser was turned on, a linear increase of the H_2O_2 signal appeared after ~10 s. Monitoring intervals of 25 s were then applied. When the diffuser was turned off, the current dropped back to the steady current level. This

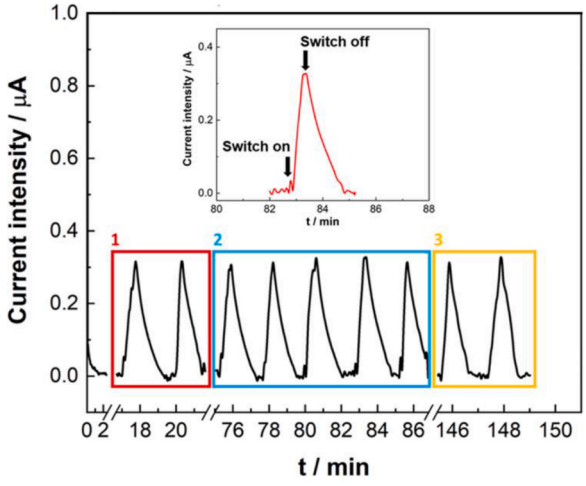

Fig. 9. Dynamic chronoamperometric response of IL/PtNi/poly(AzA) in an intermittent aerosol sample exposure system (subtracted baseline). The diffuser was loaded with 500 µM H_2O_2 in 0.1 M PB. $E_{applied}$ = 0.05 V *vs* Ag-SPCE.

process was repeated many times over more than 3 h without a loss of signal, which makes this sensor a potential option for continuous real detection of H_2O_2 in aerosol samples.

4. Conclusions

In summary, we have demonstrated a facile strategy for the synthesis of hollow-structured hybrid nanocomposites through a novel layer-by-layer approach. To do so, we alternated the electrodeposition of a conjugated polymer (polyAzure A) with electrochemical reduction of metal ions (Pt and Ni) by means of a simple one-pot method, which considerably reduces the time and complexity involved in the modification of electrodes. The composition and uniformity of the nanocomposites obtained was controlled by applying the appropriate reduction potential during manufacturing. Four reduction potentials were herein investigated for metal electrodeposition, with − 2.0 V being the optimal value. The microscopy imaging of the surfaces thus created and the electrochemical results revealed a 3D structure with Pt/Ni nanoparticles embedded in the polymeric matrix.

The present study also explored the effect of a room temperature ionic liquid confined within the porous material, with the result of enhanced electrochemical activity compared to the case with no RTIL. The sensor also showed outstanding capacity for storage over two months and for reuse by simply rinsing the modified surfaces with water. These exceptional features allowed for the continuous monitoring of H_2O_2 in aerosol phase, as well as the measurement of multiple aerosol pulses at short time intervals over more than three hours.

The notable performance of the prepared IL/PtNi/poly(AzA) nanocomposite indicates its wide range of promising applications in the field of (bio)sensors. Future work should explore the potential application of this methodology for the development of low-cost sensors for the detection of hydroperoxides in aerosols under more realistic environments and scenarios with enhanced performance.

Funding sources

Grants PID2019–106468RB-I00 and PID2019–108136RB-C32 funded by MCIN/AEI/10.13039/501100011033 and grant 2022-GRIN-34199 funded by the own research plan of the UCLM and co-financed by the European Fund for Regional Development (FEDER). RJP is the beneficiary of a postdoctoral contract associated with the first indicated project from the MCIN/AEI. This research was also partially funded by the Next-Generation EU funding (Zambrano21–10, AGB). The funders played no role in study design, in the collection, analysis and interpretation of data, in the writing of the report or in the decision to submit the article for publication.

CRediT authorship contribution statement

Rebeca Jiménez-Pérez: Conceptualization, Investigation, Methodology, Validation, Data curation, Writing – original draft, Writing – review & editing. **Jerónimo Agrisuelas:** Investigation, Methodology, Writing – original draft, Writing – review & editing. **Alicia Gomis-Berenguer:** Investigation, Methodology, Writing – original draft, Writing – review & editing. **María Teresa Baeza-Romero:** Conceptualization, Writing – review & editing, Visualization, Supervision, Project administration, Funding acquisition. **Edelmira Valero:** Conceptualization, Methodology, Validation, Writing – original draft, Writing – review & editing, Supervision, Project administration, Funding acquisition.

Declaration of Competing Interest

The authors declare that they have no known competing financial interests or personal relationships that could have appeared to influence the work reported in this paper.

Data availability

No data was used for the research described in the article.

Acknowledgements

The authors would like to acknowledge Prof. José Manuel Sevilla (University of Córdoba) and Prof. Jesús Iniesta (University of Alicante) for their helpful suggestions in the paper.

Supplementary materials

Supplementary material associated with this article can be found, in the online version, at doi:10.1016/j.electacta.2023.142683.

References

[1] H.T.H. Chan, E. Kätelhön, R.G. Compton, Voltammetry at electrodes decorated with an insulating porous film: understanding the effects of adsorption, J. Electroanal. Chem. 801 (2017) 135–140, https://doi.org/10.1016/j.jelechem.2017.07.022.
[2] A. Casanova, J. Iniesta, A. Gomis-Berenguer, Recent progress in the development of porous carbon-based electrodes for sensing applications, Analyst 147 (2022) 767–783, https://doi.org/10.1039/d1an01978c.
[3] Y. Li, J. Shi, Hollow-structured mesoporous materials: chemical synthesis, functionalization and applications, Adv. Mater. 26 (2014) 3176–3205, https://doi.org/10.1002/adma.201305319.
[4] H. v. Doan, H. Amer Hamzah, P. Karikkethu Prabhakaran, C. Petrillo, V.P. Ting, Hierarchical metal–organic frameworks with macroporosity: synthesis, achievements, and challenges, Nanomicro Lett. 11 (2019) 54, https://doi.org/10.1007/s40820-019-0286-9.
[5] W. Sebati, S.S. Ray, Advances in nanostructured metal-encapsulated porous organic-polymer composites for catalyzed organic chemical synthesis, Catalysts 8 (2018) 492, https://doi.org/10.3390/catal8110492.
[6] I. Dědek, V. Kupka, P. Jakubec, V. Šedajová, K. Jayaramulu, M. Otyepka, Metal-organic framework/conductive polymer hybrid materials for supercapacitors, Appl. Mater. Today 26 (2022), 101387, https://doi.org/10.1016/j.apmt.2022.101387.
[7] B. Bozzini, P. Bocchetta, A. Gianoncelli, Coelectrodeposition of ternary Mn-oxide/polypyrrole composites for ORR electrocatalysts: a study based on micro-X-ray absorption spectroscopy and X-ray fluorescence mapping, Energies 8 (2015) 8145–8164, https://doi.org/10.3390/en8088145 (Basel).
[8] X. Yuan, X.L. Ding, C.Y. Wang, Z.F. Ma, Use of polypyrrole in catalysts for low temperature fuel cells, Energy Environ. Sci. 6 (2013) 1105–1124, https://doi.org/10.1039/c3ee23520c.
[9] L. Torsi, M. Pezzuto, P. Siciliano, R. Relia, L. Sabbatini, L. Valli, P.G. Zambonin, Conducting polymers doped with metallic inclusions: new materials for gas sensors, Sens. Actuators B Chem. 48 (1998) 362–367, https://doi.org/10.1016/S0925-4005(98)00058-6.
[10] X. Ma, M. Gao, X. He, G. Li, Morphology tailoring of nano/micro-structured conductive polymers, composites and their applications in chemical sensors, Recent Pat NanoTechnol. 4 (2010) 150–163, https://doi.org/10.2174/187221010792483708.
[11] T. Liu, Y. Luo, J. Zhu, L. Kong, W. Wang, L. Tan, Non-enzymatic detection of glucose using poly(azure A)-nickel modified glassy carbon electrode, Talanta 156–157 (2016) 134–140, https://doi.org/10.1016/j.talanta.2016.04.053.
[12] A. Olean-Oliveira, P. Monteiro Seraphim, M.F.S. Teixeira, Methylated DNA impedimetric immunosensor based on azo-polymer-AuNPs dots and 5-methylcytosine antibody using dissolved oxygen as a redox probe, Electrochem. Commun. 136 (2022), 107242, https://doi.org/10.1016/j.elecom.2022.107242.
[13] R. Jiménez-Pérez, J. González-Rodríguez, M.-I.I. González-Sánchez, B. Gómez-Monedero, E. Valero, Highly sensitive H2O2 sensor based on poly(azure A)-platinum nanoparticles deposited on activated screen printed carbon electrodes, Sens. Actuators B Chem. 298 (2019), 126878, https://doi.org/10.1016/j.snb.2019.126878.
[14] R. Jiménez-Pérez, L. Almagro, M.I. González-Sánchez, M.Á. Pedreño, E. Valero, Non-enzymatic screen-printed sensor based on PtNPs@polyazure A for the real-time tracking of the H2O2 secreted from living plant cells, Bioelectrochemistry 134 (2020), 107526, https://doi.org/10.1016/j.bioelechem.2020.107526.
[15] R. Jiménez-Pérez, J. Iniesta, M.T. Baeza-Romero, E. Valero, On the performance of carbon-based screen-printed electrodes for (in)organic hydroperoxides sensing in rainwater, Talanta 234 (2021), 122699, https://doi.org/10.1016/j.talanta.2021.122699.
[16] B. Dalkiran, C.M.A. Brett, Polyphenazine and polytriphenylmethane redox polymer/nanomaterial–based electrochemical sensors and biosensors: a review, Microchim. Acta 188 (2021) 178, https://doi.org/10.1007/s00604-021-04821-1.
[17] M. Nasrollahzadeh, M. Sajjadi, J. Dadashi, H. Ghafuri, Pd-based nanoparticles: plant-assisted biosynthesis, characterization, mechanism, stability, catalytic and antimicrobial activities, Adv. Colloid Interface Sci. 276 (2020), 102103, https://doi.org/10.1016/j.cis.2020.102103.

[18] H. Elzanowska, E. Miasek, V.I. Birss, Electrochemical formation of Ir oxide/polyaniline composite films, Electrochim. Acta 53 (2008) 2706–2715, https://doi.org/10.1016/j.electacta.2007.08.065.
[19] T. Trung, T.H. Trung, C.S. Ha, Preparation and cyclic voltammetry studies on nickel-nanoclusters containing polyaniline composites having layer-by-layer structures, Electrochim. Acta 51 (2005) 984–990, https://doi.org/10.1016/j.electacta.2005.04.074.
[20] B. Özkale, E. Pellicer, M.A. Zeeshan, J.F. López-Barberá, J. Nogués, J. Sort, B. J. Nelson, S. Pané, One-pot electrosynthesis of multi-layered magnetic metallopolymer nanocomposites, Nanoscale 6 (2014) 4683–4690, https://doi.org/10.1039/c3nr06131k.
[21] R.M. Iost, F.N. Crespilho, Layer-by-layer self-assembly and electrochemistry: applications in biosensing and bioelectronics, Biosens. Bioelectron. 31 (2012) 1–10, https://doi.org/10.1016/j.bios.2011.10.040.
[22] A. Olean-Oliveira, G.A. Oliveira Brito, M.F.S. Teixeira, Mechanism of nanocomposite formation in the layer-by-layer single-step electropolymerization of π-conjugated Azopolymers and reduced graphene oxide: an electrochemical impedance spectroscopy study, ACS Omega 5 (2020) 25954–25967, https://doi.org/10.1021/acsomega.0c03391.
[23] R.M. Iost, J.M. Madurro, A.G. Brito-Madurro, I.L. Nantes, L. Caseli, F.N. Crespilho, Strategies of nano-manipulation for application in electrochemical biosensors, Int. J. Electrochem. Sci. 6 (2011) 2965–2997.
[24] V. Tsakova, How to affect number, size, and location of metal particles deposited in conducting polymer layers, J. Solid State Electrochem. 12 (2008) 1421–1434, https://doi.org/10.1007/s10008-007-0494-y.
[25] E. Navarro-Flores, S. Omanovic, Hydrogen evolution on nickel incorporated in three-dimensional conducting polymer layers, J. Mol. Catal. A Chem. 242 (2005) 182–194, https://doi.org/10.1016/j.molcata.2005.08.008.
[26] M. Wysocka-Zołopa, E. Grądzka, K. Szymański, K. Winkler, Electrodeposition of nickel, cobalt, and iron on polypyrrole films, Thin Solid Films 548 (2013) 44–51, https://doi.org/10.1016/j.tsf.2013.08.082.
[27] S. Srivastava, N.A. Kotov, Layer-by-layer (LBL) assembly with semiconductor nanoparticles and nanowires, Semicond. Nanocryst. Quantum Dots Synth. Assem. Spectroscopy Appl. 41 (2008) 197–216, https://doi.org/10.1007/978-3-211-75237-1_7.
[28] M. Borràs-Brull, P. Blondeau, J. Riu, The use of conducting polymers for enhanced electrochemical determination of hydrogen peroxide, Crit. Rev. Anal. Chem. 51 (2021) 204–217, https://doi.org/10.1080/10408347.2020.1718482.
[29] J. Isailović, K. Vidović, S.B. Hočevar, Simple electrochemical sensors for highly sensitive detection of gaseous hydrogen peroxide using polyacrylic-acid-based sensing membrane, Sens. Actuators B Chem. 352 (2022), 131053, https://doi.org/10.1016/j.snb.2021.131053.
[30] Ş. Sağlam, A. Üzer, R. Apak, Direct determination of peroxide explosives on polycarbazole/gold nanoparticle-modified glassy carbon sensor electrodes imprinted for molecular recognition of TATP and HMTD, Anal. Chem. 94 (2022) 17662–17669, https://doi.org/10.1021/acs.analchem.2c04450.
[31] T. Kant, K. Shrivas, I. Karbhal, S.Y Monisha, S.S Tikeshwari, Y.K. Mahipal, V. Ganesan, A graphene-printed paper electrode for determination of H_2O_2 in municipal wastewater during the COVID-19 pandemic, New J. Chem. 46 (2022) 1362–1370, https://doi.org/10.1039/D1NJ05763D.
[32] S.A. Abd Elhady, H.G.A. El-Gawad, M.F.M. Ibrahim, S. Mukherjee, A. Elkelish, E. Azab, A.A. Gobouri, R. Farag, H.A. Ibrahim, N.A. El-Azm, Hydrogen peroxide supplementation in irrigation water alleviates drought stress and boosts growth and productivity of potato plants, Sustainability 13 (2021) 899, https://doi.org/10.3390/su13020899.
[33] A.V. J.ackson, C.N. Hewitt, Atmosphere hydrogen peroxide and organic hydroperoxides: a review, Crit. Rev. Environ. Sci. Technol. 29 (1999) 175–228, https://doi.org/10.1080/10643389991259209.
[34] R.W. Noble, Q.H. Gibson, The reaction of ferrous horseradish peroxidase with hydrogen peroxide, J. Biol. Chem. 245 (1970) 2409–2413, https://doi.org/10.1016/S0021-9258(18)63167-9.
[35] M.I. González-Sánchez, B. Gómez-Monedero, J. Agrisuelas, J. Iniesta, E. Valero, Highly activated screen-printed carbon electrodes by electrochemical treatment with hydrogen peroxide, Electrochem. Commun. 91 (2018) 36–40, https://doi.org/10.1016/j.elecom.2018.05.002.
[36] A. Cuenca, J. Agrisuelas, J.J. García-Jareño, F. Vicente, Oscillatory changes of the heterogeneous reactive layer detected with the motional resistance during the galvanostatic deposition of copper in sulfuric solution, Langmuir 31 (2015) 12664–12673, https://doi.org/10.1021/acs.langmuir.5b03694.
[37] R.M. Sellers, Spectrophotometric determination of hydrogen peroxide using potassium titanium(IV) oxalate, Analyst 105 (1980) 950–954, https://doi.org/10.1039/an9800500950.
[38] T. Rapecki, M. Donten, Z. Stojek, Electrodeposition of polypyrrole-Au nanoparticles composite from one solution containing gold salt and monomer, Electrochem. Commun. 12 (2010) 624–627, https://doi.org/10.1016/j.elecom.2010.02.015.
[39] J. Agrisuelas, M.-I. González-Sánchez, E. Valero, Electrochemical properties of poly (Azure A) films synthesized in sodium dodecyl sulfate solution, J. Electrochem. Soc. 164 (2017) G1–G9, https://doi.org/10.1149/2.0201702jes.
[40] J. Agrisuelas, M.-I. González-Sánchez, B. Gómez-Monedero, E. Valero, A comparative study of poly(Azure A) film-modified disposable electrodes for electrocatalytic oxidation of H2O2: effect of doping anion, Polymers 10 (2018) 48, https://doi.org/10.3390/polym10010048 (Basel).
[41] K. Bouzek, K.M. Mangold, K. Jüttner, Platinum distribution and electrocatalytic properties of modified polypyrrole films, Electrochim. Acta 46 (2001) 661–670, https://doi.org/10.1016/s0013-4686(00)00659-9.
[42] S.B. Emery, J.L. Hubbley, D. Roy, Voltammetric and amperometric analyses of electrochemical nucleation: electrodeposition of copper on nickel and tantalum, J. Electroanal. Chem. 568 (2004) 121–133, https://doi.org/10.1016/j.jelechem.2004.01.012.
[43] A.C. Fortuin, C. Jackson, E. Carleschi, B.P. Doyle, A. Shnier, R.J. Kriek, S.C. Ray, D. G. Billing, D. Wamwangi, G.G. Scherer, P.B.J. Levecque, Towards practical applications of EQCN experiments to study Pt anchor sites on carbon surfaces, Electrocatalysis 9 (2018) 271–278, https://doi.org/10.1007/s12678-017-0430-6.
[44] B.M. Hryniewicz, J. Volpe, L. Bach-Toledo, K.C. Kurpel, A.E. Deller, A.L. Soares, J. M. Nardin, L.F. Marchesi, F.F. Simas, C.C. Oliveira, L. Huergo, D.E.P. Souto, M. Vidotti, Development of polypyrrole (nano)structures decorated with gold nanoparticles toward immunosensing for COVID-19 serological diagnosis, Mater. Today Chem. 24 (2022), 100817, https://doi.org/10.1016/j.mtchem.2022.100817.
[45] L.F. Marchesi, S.C. Jacumasso, R.C. Quintanilha, H. Winnischofer, M. Vidotti, The electrochemical impedance spectroscopy behavior of poly(aniline) nanocomposite electrodes modified by Layer-by-Layer deposition, Electrochim. Acta 174 (2015) 864–870, https://doi.org/10.1016/j.electacta.2015.05.077.
[46] E.P. Randviir, A cross examination of electron transfer rate constants for carbon screen-printed electrodes using Electrochemical Impedance Spectroscopy and cyclic voltammetry, Electrochim. Acta 286 (2018) 179–186, https://doi.org/10.1016/j.electacta.2018.08.021.
[47] L. Rimoldi, V. Pifferi, D. Meroni, G. Soliveri, S. Ardizzone, L. Falciola, Three-dimensional mesoporous silica networks with improved diffusion and interference-abating properties for electrochemical sensing, Electrochim. Acta 291 (2018) 73–83, https://doi.org/10.1016/j.electacta.2018.08.131.
[48] C.P. McCord, B. Summers, C.S. Henry, Redox behavior and surface morphology of polystyrene thermoplastic electrodes, Electrochim. Acta 393 (2021), 139069, https://doi.org/10.1016/j.electacta.2021.139069.
[49] K.-C. Pham, D.S. McPhail, C. Mattevi, A.T.S. Wee, D.H.C. Chua, Graphene-carbon nanotube hybrids as robust catalyst supports in proton exchange membrane fuel cells, J. Electrochem. Soc. 163 (2016) F255–F263, https://doi.org/10.1149/2.0891603jes.
[50] J. Wang, Q. Zhao, H. Hou, Y. Wu, W. Yu, X. Ji, L. Shao, Nickel nanoparticles supported on nitrogen-doped honeycomb-like carbon frameworks for effective methanol oxidation, RSC Adv. 7 (2017) 14152–14158, https://doi.org/10.1039/C7RA00590C.
[51] P. Dubey, N. Kaurav, R.S. Devan, G.S. Okram, Y.K. Kuo, The effect of stoichiometry on the structural, thermal and electronic properties of thermally decomposed nickel oxide, RSC Adv. 8 (2018) 5882–5890, https://doi.org/10.1039/C8RA00157J.
[52] M.M. Barsan, E.M. Pinto, C.M.A. Brett, Methylene blue and neutral red electropolymerisation on AuQCM and on modified AuQCM electrodes: an electrochemical and gravimetric study, Phys. Chem. Chem. Phys. 13 (2011) 5462–5471, https://doi.org/10.1039/c1cp20418a.
[53] J. Agrisuelas, J.J. García-Jareño, D. Gimenez-Romero, F. Vicente, An approach to the electrochemical activity of poly-(phenothiazines) by complementary electrochemical impedance spectroscopy and Vis-NIR spectroscopy, Electrochim. Acta 55 (2010) 6128–6135, https://doi.org/10.1016/j.electacta.2009.12.092.
[54] R. Jiménez-Pérez, J.M. Sevilla, T. Pineda, M. Blázquez, J. Gonzalez-Rodriguez, Electrocatalytic performance enhanced of the electrooxidation of gamma-hydroxybutyric acid (GHB) and ethanol on platinum nanoparticles surface. A contribution to the analytical determination of GHB in the presence of ethanol, Sens. Actuators B Chem. 256 (2018) 553–563, https://doi.org/10.1016/j.snb.2017.10.142.
[55] J. Agrisuelas, A. Cuenca, A. Frau, D. Ferrús, J.J. García-Jareño, R. Sanchis-Gual, F. Vicente, Ageing effect on the electrochemical properties in poly(Azure A) films, J. Electrochem. Soc. 164 (2017) H593–H602, https://doi.org/10.1149/2.0791709jes.
[56] S. Zhang, J. Zhang, Y. Zhang, Y. Deng, Nanoconfined ionic liquids, Chem. Rev. 117 (2017) 6755–6833, https://doi.org/10.1021/acs.chemrev.6b00509.
[57] C. Largeot, C. Portet, J. Chmiola, P.-L. Taberna, Y. Gogotsi, P. Simon, Relation between the ion size and pore size for an electric double-layer capacitor, J. Am. Chem. Soc. 130 (2008) 2730–2731, https://doi.org/10.1021/ja7106178.
[58] C. Merlet, C. Péan, B. Rotenberg, P.A. Madden, B. Daffos, P.L. Taberna, P. Simon, M. Salanne, Highly confined ions store charge more efficiently in supercapacitors, Nat. Commun. 4 (2013) 1–6, https://doi.org/10.1038/ncomms3701.
[59] E.H. Lahrar, A. Belhboub, P. Simon, C. Merlet, Ionic liquids under confinement: from systematic variations of the ion and pore sizes toward an understanding of the structure and dynamics in complex porous carbons, ACS Appl. Mater. Interfaces 12 (2020) 1789–1798, https://doi.org/10.1021/acsami.9b16740.
[60] S. Kondrat, N. Georgi, M.v. Fedorov, A.A. Kornyshev, A superionic state in nano-porous double-layer capacitors: insights from Monte Carlo simulations, Phys. Chem. Chem. Phys. 13 (2011) 11359, https://doi.org/10.1039/c1cp20798a.
[61] S. Kondrat, A. Kornyshev, Superionic state in double-layer capacitors with nanoporous electrodes, J. Phys. Condens. Matter 23 (2011), 022201, https://doi.org/10.1088/0953-8984/23/2/022201.
[62] F. Borghi, C. Piazzoni, M. Ghidelli, P. Milani, A. Podestà, Nanoconfinement of ionic liquid into porous carbon electrodes, J. Phys. Chem. C 125 (2021) 1292–1303, https://doi.org/10.1021/acs.jpcc.0c08145.
[63] D. Gurina, E. Odintsova, A. Kolesnikov, M. Kiselev, Y. Budkov, Disjoining pressure of room temperature ionic liquid in charged slit carbon nanopore: molecular

dynamics study, J. Mol. Liq. 366 (2022), 120307, https://doi.org/10.1016/j.molliq.2022.120307.
[64] R. Atkin, N. Borisenko, M. Drüschler, F. Endres, R. Hayes, B. Huber, B. Roling, Structure and dynamics of the interfacial layer between ionic liquids and electrode materials, J. Mol. Liq. 192 (2014) 44–54, https://doi.org/10.1016/j.molliq.2013.08.006.
[65] G.M. Eisenberg, Colorimetric determination of hydrogen peroxide, Ind. Eng. Chem. Anal. Ed. 15 (1943) 327–328, https://doi.org/10.1021/i560117a011.